NANO LETTERS

LETTER

pubs.acs.org/NanoLett

Visualizing Gold Nanoparticle Uptake in Live Cells with Liquid Scanning Transmission Electron Microscopy

Diana B. Peckys and Niels de Jonge*

Department of Molecular Physiology and Biophysics, Vanderbilt University Medical Center, Nashville, Tennessee 37232, United States

ABSTRACT: The intracellular uptake of 30 nm diameter gold nanoparticles (Au-NPs) was studied at the nanoscale in pristine eukaryotic cells. Live COS-7 cells were maintained in a microfluidic chamber and imaged using scanning transmission electron microscopy. A quantitative image analysis showed that Au-NPs bound to the membranes of vesicles, possibly lysosomes, and occupied 67% of the available surface area. The vesicles accumulated to form a micrometer-sized cluster after 24 h of incubation. Two clusters were analyzed and found to consist of 117 ± 9 and 164 ± 4 NP-filled vesicles.

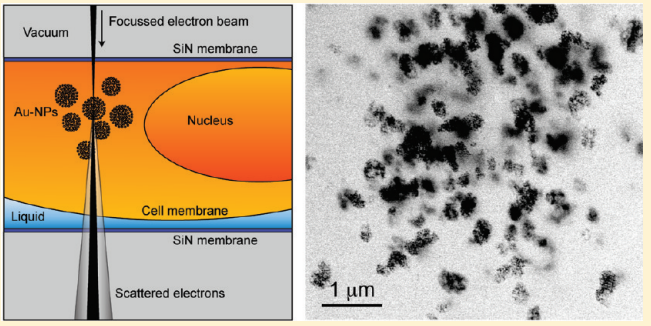

KEYWORDS: Biological electron microscopy, live cells, scanning transmission electron microscopy, STEM, gold nanoparticles, nanotoxicology, nanoparticle uptake

Conjugated nanoparticles (NPs) join distinct nanoscale properties with specific surface bound ligands, a combination that has led to widespread applications in diagnostics and therapeutics.[1−4] NPs can for instance be used as efficient contrast agents for molecular imaging,[5] as carriers for targeted drug[6] and gene delivery,[7] and as therapeutical reagents for targeted photothermal therapy.[8,9] Cytotoxicological studies of NPs are a major part of the assessment of NPs for medical applications and include the visualization and characterization of in vitro NP uptake.[10−13] NP uptake is influenced by many factors, such as NP size, shape, surface chemistry, colloidal stability, nonspecific interactions, and cell line.[14−20] Imaging studies provide crucial information on NP−cell interactions, especially on the intracellular trafficking and fate of NPs and on their incorporated quantity.[21−23] Single NPs cannot be resolved with light microscopy, for that reason, electron microscopy (EM) is used to record high-resolution images of intracellular NPs. Unfortunately, the sample preparation for EM typically includes processing of samples into 50−200 nm thin sections, a step that involves the risk of NP removal. A further disadvantage is the difficulty to quantitatively evaluate NP uptake from conventional EM images, since thin sections may be cut through three-dimensional structures, such as vesicles with high densities of NPs.

Here, we present a new approach for the study of NP−cell interactions. Live fibroblast cells (COS-7) loaded with Au-NPs were imaged in liquid with scanning transmission electron microscopy (STEM) using a microfluidic chamber[24,25] that provided a continuous flow of buffer. STEM images were recorded through the transparent windows of the chamber; see Figure 1. The cells were alive at the onset of STEM imaging, and the obtained images thus provide information about the NP distribution in pristine cells. This EM approach can be used to study cells of up to ∼10 μm thickness, excluding the need for sectioning and requiring only a minimal sample preparation.

The microfluidic chamber was made from two silicon microchips, each having a 50 nm thin silicon nitride (SiN) membrane in their center,[25] providing transparent windows for photons and electrons at the energies used in this study. At the same time, the SiN membranes enclosed the liquid in the chamber and thus sealed the cells from the vacuum in the electron microscope. The dimensions of the SiN membranes were 50 × 200 μm or 50 × 400 μm. One microchip had a flat surface and was used as substrate for the adhering cells; the second microchip had a 6 μm thick spacer in parallel with the two long sides. This spacer prevented compression of the cells when both microchips were assembled into a microfluidic chamber. The microchips were cleaned, and coated as previously described.[24] Briefly, the flat microchips (without spacer) were rinsed in acetone followed by a rinse in ethanol (both from Sigma Aldrich) and then ambient air plasma cleaned. To promote attachment of the COS-7 cells, a coating with poly-L-lysine (PLL) (Sigma Aldrich) was applied.

The COS-7 cells (green monkey kidney fibroblast, from ATTC) were grown in Dulbecco's Modified Eagle's Medium (ATTC), with 10% fetal bovine serum (Invitrogen), at 37 °C in a 5% CO_2 environment. To grow cells directly on the microchips, the cells were harvested upon ∼90% confluency by rinsing the adherent cell layer with $Ca^{2+/}Mg^{2+}$ free Dulbecco's phosphate buffered saline (GIBCO), incubating the cells with cell stripper solution (MediaTech) and subsequent quenching and suspension in the medium. One droplet of cell suspension was added per PLL-coated microchip. Once a sufficient number of cells (3−12) had settled down on the SiN membrane, usually after a

Received: January 25, 2011
Revised: February 23, 2011
Published: March 16, 2011

few minutes, the microchips were transferred into new medium and incubated overnight at 37 °C in a 5% CO_2 environment.

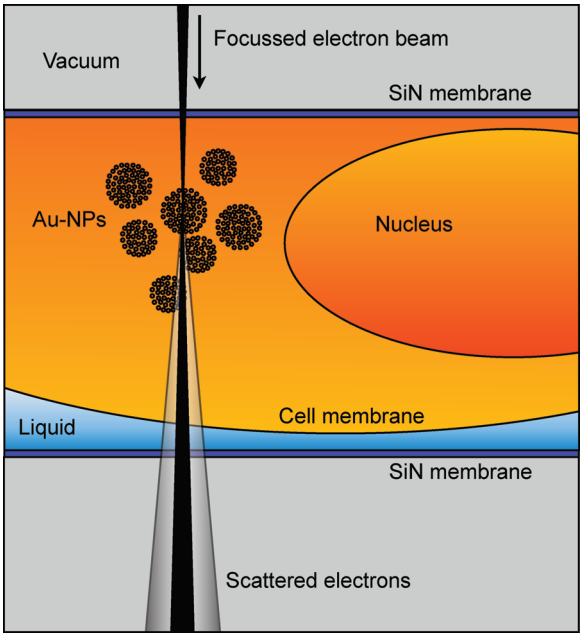

Figure 1. Principle of liquid scanning transmission microscopy (STEM) of live eukaryotic cells. A cell (orange) is enclosed in a microfluidic chamber between two 50 nm thin silicon nitride membranes supported by silicon microchips, protecting the cell from the vacuum (gray) inside the STEM. Gold nanoparticles (Au-NPs) accumulate in clusters of Au-NP-filled vesicles. Continuous flow of buffer (blue) keeps the cell alive until scanning with the electron beam (black) is started.

To ensure that the cells could be kept alive inside the microfluidic chamber, we first examined the cell survival in the chamber, independently of the recording of STEM images. Cells that had settled on microchips overnight were incubated for 1 h with the live/dead indicator calcein AM (Invitrogen), 1 μM in Tyrode's buffer (TB) (Sigma Aldrich). Calcein AM is an initially nonfluorescent, cell permeable compound that is converted into green fluorescent calcein when hydrolyzed by intracellular esterases in live cells. To enclose the cells in a microfluidic chamber, two microchips, one with cells and one with spacer, were assembled in the liquid flow EM specimen holder (Protochips Inc.). First, the dry microchip with spacer was placed in the slot for the microchips in the tip of the holder, with the spacer side up. The wet microchip with adhering cells upside down was placed (rapidly to prevent drying) on the spacer microchip. Due to the design of the slot, this "sandwiching" procedure aligned the microchips with a precision of 20 μm such that their SiN windows overlapped to a degree of at least 80%, providing visibility of the cells enclosed between the membranes. The microfluidic compartment was closed with a lid, and the flow of the imaging buffer (1 μM Calcein AM in TB) was initiated. The total assembly time amounted to 1−2 min.

The cells were imaged with an inverted fluorescence microscope (Nikon Diaphot 300), equipped with 20× (Nikon Plan 20/0.40 phase 2 160/1.2) and 40× (Nikon Plan 40/0.55 phase 3 160/0−2.5) air lenses and an EXFO X-Cite 120PC XL illumination system that included a 120 W mercury arc lamp. The fluorescence image of Figure 2a shows the cells on a microchip before enclosure. Figure 2b is the same sample in a closed chamber, ∼2 min after assembly. Figure 2c was taken 40 min after the microfluidic chamber had been reopened; the cells were enclosed for 4 mins total. None of the cells displayed signs of damage. Several other samples were tested as well. Cells in the

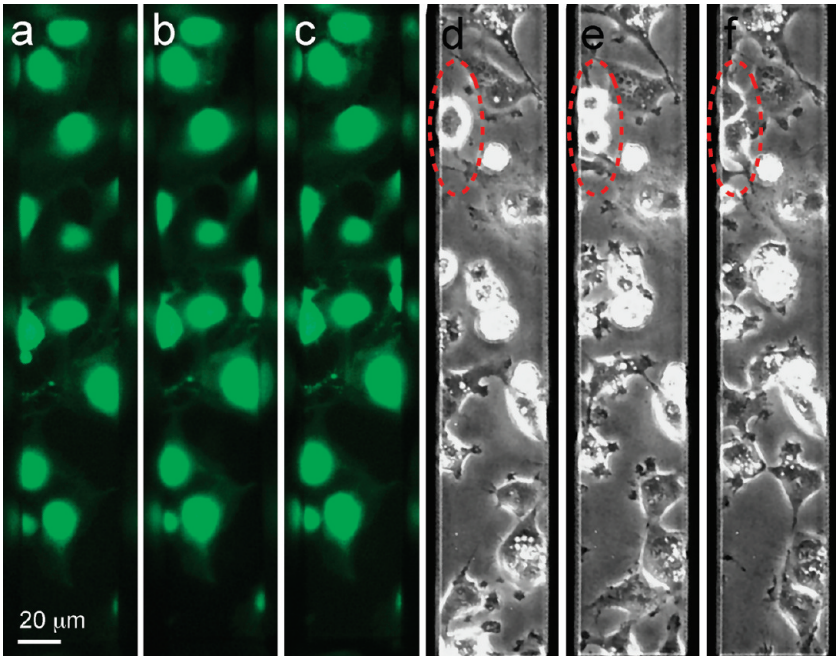

Figure 2. Assessment of cell viability. (a) Fluorescence microscopy of live COS-7 cells on a microchip. The cells were stained with the live/dead indicator calcein AM (green fluorescence indicates undamaged membrane integrity). (b) The same cells 2 min after enclosure in a microfluidic chamber. (c) The cells after opening of the microfluidic chamber 40 min later. (d) Phase contrast image of a different sample of live COS-7 cells 39 h after opening of the microfluidic chamber. The dotted oval in the upper left image area indicates the cell that underwent mitosis. (e, f) Cells division occurring in a time period of 2 h.

dx.doi.org/10.1021/nl200285r |*Nano Lett.* 2011, 11, 1733–1738

microfluidic chamber kept their calcein fluorescence intensity unchanged for the maximal tested time period of 2.5 h, indicating that the cells were alive for at least 2.5 h in the microfluidic chamber. Note that the cells lost their viability in the chamber within 15 min without the flow of buffer.

To examine if the enclosing process caused delayed cellular damage, we inspected several samples for cell division, i.e., mitosis, the occurrence of which is the most stringent criterion of cell viability. Because mitosis is temperature dependent and the liquid flow holder had no internal heater, we reopened the microfluidic chamber and placed the microchip with the cells in a dish filled with CO_2-independent medium (Invitrogen). The dish was transferred onto the stage of the microscope, equipped with an environmental system to ensure a constant temperature of 37 °C and 100% humidified air. The total time the samples spent in the microfluidic chamber was reduced to 4 min, because the cells adhered to the spacer microchip after 5 min, causing cell rupture upon opening of the microfluidic chamber. During the following 53 h, a time-lapse series of phase-contrast images was recorded with 3 min intervals, revealing three mitosis events at the location of the SiN window. A mitosis that happened after 39 h is shown in the area of the dotted oval in Figure 2d–f. Cells were also tested for signs of programmed cell death,[26] i.e., apoptosis, by incubating the samples for 30 min in Hoechst 33342 (Invitrogen), 1 μg/mL in TB, a nuclear fluorescent stain. None of the tested cells had developed signs of programmed cell death 53 h after opening of the microfluidic chamber. Similar results were obtained for two further samples. Cells kept in the microfluidic chamber were thus viable following the most stringent criterion of viability, namely, mitosis.

After we had ensured that it was possible to keep the COS-7 cells alive and intact in the microfluidic chamber, we conducted STEM experiments to study the fate of NPs taken up by COS-7 cells. Microchips with adherent cells were serum-starved for 2 h to enhance the following uptake of serum protein coated Au-NPs.[27] Thirty nanometer diameter unconjugated Au-NPs (Ted Pella) were coated with serum proteins by mixing 0.5 mL of the Au-NP stock solution with 2 mL of 10% FBS supplemented medium and subsequent incubation at 40 °C under rotation (30 rpm), for 2 h. Such serum protein coating has been shown to prevent clustering of the Au-NPs and to favor their endocytotic uptake.[17] The Au-NP solution was centrifuged for 6 min at 5000g and the pellet was dissolved in 10% FBS supplemented medium, to yield a final volume of 60 μL with an Au-NP concentration of ~1.8 nM. Twelve microliter droplets of this Au-NP solution were placed against the inner rim of cutoff PCR tube lids. Microchips with serum-starved cells were individually placed in an inclined orientation against a droplet, such that the cells were submerged and upside down in the Au-NP solution and incubated for 2 h in a humid environment, at 37 °C in the CO_2 incubator. Subsequently, the samples were rinsed and incubated overnight in 10% FBS supplemented medium, at 37 °C in the CO_2 incubator. After 24 h, the cells were enclosed in the microfluidic chamber.

Imaging with liquid STEM took place within 3 min after enclosure. The STEM (CM200, FEI Company, Oregon) was set to 200 kV, a beam semiangle α of 9 mrad, a pixel dwell time of 20 μs, a probe current of 0.16 nA, a magnification of 16000, a pixel size of 8.7 nm, an image size of 1024 × 1024 pixels (representing sample areas of 8.8 × 8.8 μm^2), and an annular dark field detector semiangle of 70 mrad. Panels a and b of Figure 3 show selected cell areas of 4.9 × 4.9 μm^2 (Figure 3a) 7.4 × 7.4 μm^2 (Figure 3b), depicting two representative intracellular clusters that consisted

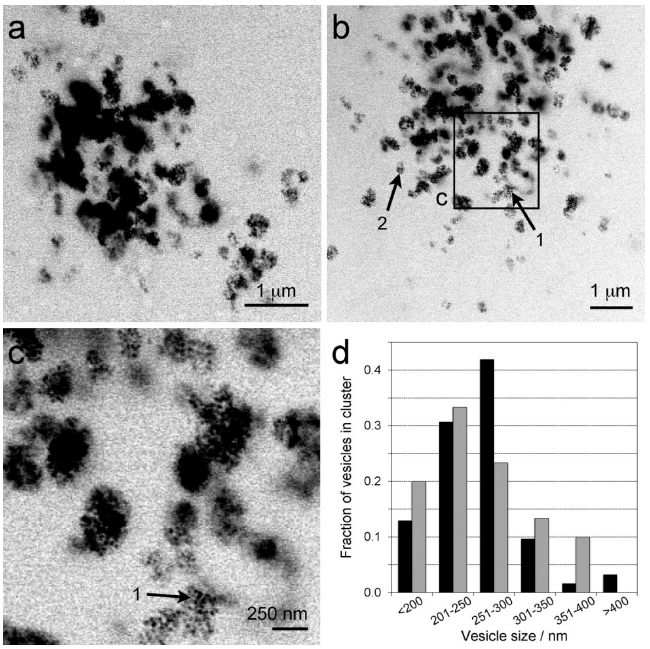

Figure 3. STEM of live cells in a microfluidic chamber, 24 h after incubation with Au-NPs. (a, b) Images of intracellular Au-NP aggregations in two different cells, illustrating that Au-NPs had concentrated in three-dimensional clusters of vesicles densely filled with Au-NPs. (c) Detail of panel b showing the distribution of single NPs. Blurred Au-NPs are located outside the focus plane and illustrate the highly three-dimensional arrangement of the structures. (d) Normalized size distribution histogram of Au-NP filled vesicles shown in panel a (gray) and panel b (black).

of vesicles with Au-NPs, appearing as dark spots. The average diameter of this type of cluster was measured from light microscopy images and was 4.6 ± 1 μm (n = 25), where the variation represents the standard measured sizes, and the measurement accuracy was 0.5 μm. The STEM images revealed that each cluster contained more than hundred round structures that were densely filled with Au-NPs. Due to their approximate round shapes and their filling with Au-NPs, we suggest that these structures are vesicles. Figure 3c is a detail of Figure 3b highlighting the distribution of single NPs inside the vesicles. The STEM images display the Au-NP-filled vesicles with different degrees of sharpness; this indicates that they were not on the same focal plane, but scattered over several micrometers in depth. The sharpest NP images can be found when these are in the focal plane and at a vertical location close to the top window, where the electron beam enters the sample. The electron probe is blurred toward layers deeper in the specimen due to a combination of geometric broadening and beam broadening on account of interactions of the electron beam with the specimen. A fraction of 63% of the probe current was scattered into the opening angle of the detector, from which we calculated the thickness of the liquid[24] to be 10 ± 2 μm. The Au-NPs appear as black spots on account of this large liquid thickness, leading to a contrast reversal. For thinner liquids the Au-NPs appear as bright spots. The liquid thickness was thicker than what was expected on the basis of the spacer of 6 μm, and can be explained by a bulging of the SiN windows outward into the vacuum.[25]

STEM imaging of pristine cells is subject to radiation damage. Yet, the STEM images do not show signs of severe damage. The majority of the Au-NP-filled vesicles in Figure 3 had round or

dx.doi.org/10.1021/nl200285r |Nano Lett. 2011, 11, 1733–1738

oval shapes, and the pattern of intravesicular Au-NPs appeared homogeneous. The cells were exposed to 2×10^4 electrons per scan pixel of a size of 8.7 nm, and the average electron dose was thus 3 $e^-/Å^2$. The electron dose was a factor of 10 above the dose limit for EM above which subnanometer structural features become damaged in wet biological specimens,[28] and a factor of 10 below the corresponding limit used in cryo-EM.[29] Note that the local electron dose directly in the focal plane was higher, maximal 1.6×10^2 $e^-/Å^2$ (for a diameter of the electron probe containing 50% of the current of 0.9 nm). But, only a small region of a cell was exposed to the higher dose, because electron beam scanning occurred with lines separated by the pixel size of 9 nm, and beam broadening rapidly decreases the radiation intensity in deeper layers.[30] The absence of signs of severe radiation damage in the images and the fact that the average electron dose was smaller than the dose used in cryo-EM lead to the hypothesis that the first image recorded on a cell can be used to assess the distribution of NPs inside a live cell.

Figure 3 shows that the Au-NP filled endocytotic vesicles had accumulated into a large cluster. Similar conglomerations of NP-filled vesicles have been reported for several types of NPs in the vicinity of the endosomal recycling compartment (ERC), a perinuclear organelle involved in endosome recycling.[19,31−33] To determine the number of Au-NP-filled vesicles per cluster, the original STEM images were analyzed, of which selected areas are shown in panels a and b of Figure 3. Vesicles were visually identified and counted if their contrast exceeded the background gray value by at least 30% and if their size was >100 nm. The counting was repeated four times per image resulting in a total of 117 ± 9 (cluster of Figure 3a) and 164 ± 4 (cluster of Figure 3b) NP-filled vesicles. We cannot exclude that several NP-filled vesicles might have been located outside the image area; therefore these numbers represent minimum values. This applies particularly for the cluster shown in Figure 3a, because beam blurring possibly prevented the identification of additional vesicles.

From vesicles that were in or close to the focal plane, we measured the average diameter to be 0.26 ± 0.05 μm (n = 63, Figure 3b; n = 30, Figure 3a). The diameters were measured from the STEM images using Image J (NIH). The distribution of vesicle sizes is depicted in Figure 3d and shows a maximum for vesicle diameters between 200 and 300 nm in both analyzed clusters. This size distribution histogram is similar to the size distribution of lysosomes.[34,35] Since the endocytotic pathway shuttles cargo from vesicles to early endosomes to late endosomes/multivesicular bodies and finally, for degradation, to lysosomes, we propose that 24 h after their intracellular uptake the Au-NPs had ended up in lysosomes.

To assess the distribution of Au-NPs within the vesicles, we counted the Au-NPs in selected vesicular regions of 17 × 17 pixels (150 × 150 nm^2). Figure 4a shows an example that represents such an area from the vesicle at arrow #1 in Figure 3b. Figure 4b shows a line-scan over a region with darker pixels, presumed to represent an Au-NP, having a full width at half-maximum of 28 ± 5 nm, which corresponds to the 30 nm diameter of the Au-NPs. Individual NPs can thus be recognized but the image is so pixelated that Au-NP counting is difficult. To facilitate the counting of NPs, the image in Figure 3b was processed with Image J (NIH), first by enlargement of a factor of 10 and then by filtering with Gaussian blur with a radius of 1.5 pixels. In the filtered image of Figure 4c the NPs can be recognized better than in the original image. In this example, a total of 12 Au-NPs was counted as indicated by the circles. An

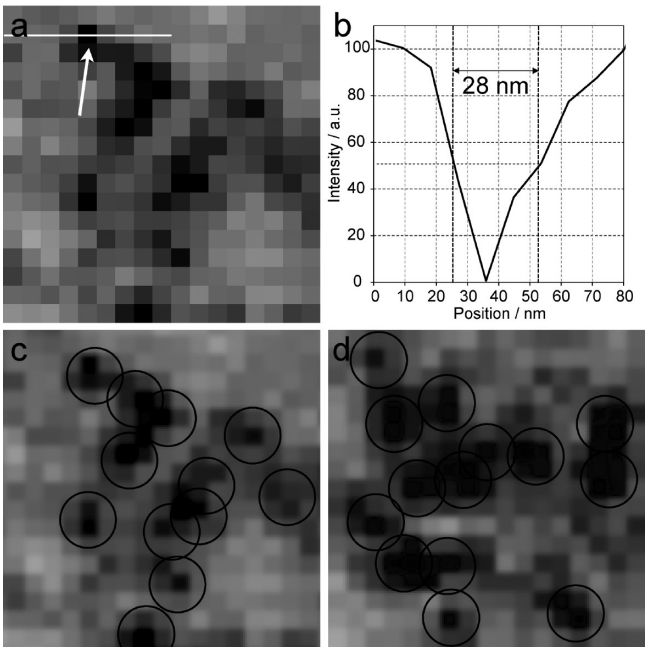

Figure 4. STEM image analysis to determine the density of Au-NPs in vesicles. (a) Selected region of 17 × 17 pixels at arrow #1 in Figure 3b. (b) A line scan was drawn over a darker region assumed to represent an Au-NP in (a) (see arrow). The full width at half-minimum was 28 ± 5 nm. (c) Filtered image used for the counting of Au-NPs (circles). (d) Selected region at arrow #2 in Figure 3b displaying 14 Au-NPs.

example from another region is shown (image processed) in Figure 4d (arrow #2 in Figure 3b); here, we counted 14 Au-NPs. A total of 25 of such image sections were placed over vesicles and analyzed and yielded an average of 12 ± 2 Au-NPs.

The degree of overlap of Au-NPs in these vesicular image areas was sufficiently low, such that we could identify and count individual NPs, and we found a homogeneous distribution of the Au-NPs throughout the analyzed areas. This distribution points toward localization of the NPs at the membrane of the lysosomes, rather than to a complete filling of the entire intravesicular space. If this entire space would have been filled, we would expect to see a higher density of Au-NPs in the central parts of the vesicles compared to the periphery, which was not the case. The degree of coverage of the vesicle membrane by Au-NPs was determined as follows. The surface area of an average-sized vesicle was 0.21 ± 0.07 μm^2 assuming a spherical shape. A 30 nm large gold sphere with a 5 nm thick layer of bound serum protein yields an effective Au-NP diameter of 40 nm. On account of the curvature of the inner vesicle surface and assuming a monolayer of tightly packed Au-NPs, a single Au-NP would occupy an area of ~50 × 50 nm^2, and the theoretical maximum density is thus 400 Au-NPs/μm^2 on the inner vesicle surface. Consequently, an average vesicle could hold a maximum of 85 ± 30 Au-NPs (Table 1). The actual number of Au-NPs in an image, projecting both the upper and lower halves of a vesicle, was 12 ± 2 in an area of 2 × 0.15 × 0.15 = 0.045 μm^2. The actual density at the inner vesicle surface was thus 267 ± 44 Au-NPs/μm^2, and a vesicle contained an average 57 ± 26 Au-NPs, which corresponds to 67 ± 11% occupancy of the available membrane area. The total number of Au-NPs in the lysosome cluster was estimated to be $(9 \pm 5) \times 10^3$.

The finding that Au-NPs are bound to the inner vesicular surface is supported by some studies of Au-NPs in intracellular

dx.doi.org/10.1021/nl200285r |Nano Lett. 2011, 11, 1733–1738

Table 1. Quantitative Analysis of Au-NP Distribution[a]

number of vesicles in cluster	164* ± 4
vesicle diameter (μm)	0.26* ± 0.05
estimated vesicle surface area (μm^2)	0.21 ± 0.07
number of detected Au-NPs per 0.15 × 0.15 μm^2 of image	12* ± 2
density of Au-NPs/μm^2 on vesicle membrane	267 ± 44
number of Au-NPs/vesicle	57 ± 26
theoretical max. number of Au-NPs/vesicle	85 ± 30
theoretical max. density of Au-NPs/μm^2 on vesicle membrane	400 Au-NPs/μm^2
occupancy of available vesicle membrane area	67 ± 11%
total number of Au-NPs in vesicle cluster	(9 ± 5) × 10^3

[a] Values marked with an astereisk were directly determined from the STEM image of Figure 3b.

vesicles using conventional EM images.[20] However, there is a controversy about such a vesicular membrane bound location, and several other published EM images show intravascular NPs that form aggregates in the vesicles.[13,36,37] In addition, EM images often depict only a few NPs per vesicle,[18,37−39] possibly underestimating the occupancy of the available area by NPs. These discrepancies in the location and in the amount of vesicular NPs might relate to concerns about the sectioning of EM samples.[21] First, one cannot be sure where a vesicle was cut through, which complicates quantitative studies. Second, EM sample preparation is prone to introduce artifacts[40] hindering quantification in NP uptake studies. The issue of artifacts is multifaceted. NPs may become displaced by the diamond knife,[41] or may be washed away during sample preparation. Cell fixation can redistribute NPs coated with cell-penetrating peptides into the nucleus,[42] and translocate NPs with positively charged proteins across the cell membrane.[43] Staining can introduce electron-dense nanosized aggregates that are difficult to distinguish from the NPs under investigation.[36,44] Third, with conventional EM it is almost impossible to conduct a quantitative study on the scale of the entire cluster of vesicles. In order to do so, many images from a large number of sections would have to be analyzed.[45]

Liquid STEM, on the contrary, achieves single NP resolution on fully hydrated, nonfixed, intact cells that are living at the onset of imaging. The images contain signals from the full three-dimensional space of the cell, which can be used for quantitative studies of NP uptake and spatial distribution as demonstrated in this work. The whole cell analysis can be done on a much faster time scale (hours versus days) than possible with conventional EM,[41] making the STEM approach suitable for routine measurements, needed for instance when systematic variations of NP materials and surface coating are included in the uptake study.[21] The biological structure of the cells cannot be visualized with high resolution using electron microscopy of whole cells in liquid, because the contrast obtained on the carbon-based materials within water is too low. The cellular structure may be visualized using fluorescent probes and light microscopy, which can be correlated with the STEM images. Future studies on cell−NP interactions may well include such a fluorophore labeling to identify specific proteins and pathways that participate in NP uptake, trafficking, storage, and exocytosis, by light microscopy prior to STEM imaging.

We studied the intracellular uptake of 30 nm diameter Au-NPs in COS-7 cells with liquid STEM. The spatial distribution of NPs was determined in fully hydrated, pristine cells that were alive at the onset of imaging. On account of the absence of preparation of the cells into thin sections standard in EM, we were able to conduct a quantitative analysis of the NP distribution. The NPs were located in vesicles, possibly lysosomes. A total of 117 ± 9 and 164 ± 4 vesicles were found in two analyzed clusters after 24 h of incubation. The NPs were bound to the membranes of the vesicles, with 57 ± 26 Au-NPs/vesicle. About 67% of the available membrane surface area was covered with NPs. The total number of Au-NPs in the vesicle cluster was (9 ± 5) × 10^3. We propose that liquid STEM of live cells can be used for quantitative studies of NP−cell interactions.

AUTHOR INFORMATION

Corresponding Author
*E-mail: niels.de.jonge@vanderbilt.edu.

ACKNOWLEDGMENT

We thank T. E. McKnight, P. Mazur, D. W. Piston, and Protochips, Inc., NC. STEM images were recorded at the SHaRE User Facility, sponsored by the Division of Scientific User Facilities, Office of Basic Energy Sciences, U.S. Department of Energy. Research was supported by Vanderbilt University Medical Center and by NIH Grants R01RR018470 (to P. Mazur) and 1R43EB008589 (to S. Mick).

REFERENCES

(1) Petros, R. A.; DeSimone, J. M. *Nat. Rev. Drug Discovery* **2010**, *9*, 615–627.
(2) Michalet, X.; Pinaud, F. F.; Bentolila, L. A.; Tsay, J. M.; Doose, S.; Li, J. J.; Sundaresan, G.; Wu, A. M.; Gambhir, S. S.; Weiss, S. *Science* **2005**, *307*, 538–544.
(3) McCarthy, J. R.; Weissleder, R. *Adv. Drug Delivery Rev.* **2008**, *60*, 1241–1251.
(4) Liong, M.; Lu, J.; Kovochich, M.; Xia, T.; Ruehm, S. G.; Nel, A. E.; Tamanoi, F.; Zink, J. I. *ACS Nano* **2008**, *2*, 889–896.
(5) Weissleder, R.; Pittet, M. J. *Nature* **2008**, *452*, 580–589.
(6) Kim, C. K.; Ghosh, P.; Rotello, V. M. *Nanoscale* **2009**, *1*, 61–67.
(7) Whitehead, K. A.; Langer, R.; Anderson, D. G. *Nat. Rev. Drug Discovery* **2009**, *8*, 129–138.
(8) Lal, S.; Clare, S. E.; Halas, N. J. *Acc. Chem. Res.* **2008**, *41*, 1842–1851.
(9) Huang, X.; Jain, P. K.; El-Sayed, I. H.; El-Sayed, M. A. *Lasers Med. Sci.* **2008**, *23*, 217–228.
(10) Ma, Y. *In Vitro Models for Nanotoxicity Testing.*; John Wiley & Sons, Ltd.: New York, 2009; pp 349−377.
(11) Lanone, S.; Boczkowski, J. *Curr Mol Med* **2006**, *6*, 651–663.
(12) Monteiro-Riviere, N. A.; Tran, C. L. *Nanotoxicology: characterization, dosing and health effects*; Informa Healthcare USA, Inc.: New York, 2007.
(13) Mukherjee, P.; Bhattacharya, R.; Bone, N.; Lee, Y. K.; Patra, C. R.; Wang, S.; Lu, L.; Secreto, C.; Banerjee, P. C.; Yaszemski, M. J.; Kay, N. E.; Mukhopadhyay, D. *J. Nanobiotechnol.* **2007**, *5*, 4.
(14) Verma, A.; Stellacci, F. *Small* **2010**, *6*, 12–21.
(15) Hardman, R. *Environ. Health Perspect.* **2006**, *114*, 165–172.
(16) Chithrani, B. D.; Chan, W. C. *Nano Lett.* **2007**, *7*, 1542–1550.
(17) Chithrani, B. D.; Ghazani, A. A.; Chan, W. C. *Nano Lett.* **2006**, *6*, 662–668.
(18) Jiang, W.; Kim, B. Y.; Rutka, J. T.; Chan, W. C. *Nat. Nanotechnol.* **2008**, *3*, 145–150.
(19) Barua, S.; Rege, K. *Small* **2009**, *5*, 370–376.
(20) Mironava, T.; Hadjiargyrou, M.; Simon, M.; Jurukovski, V.; Rafailovich, M. H. *Nanotoxicology* **2010**, *4*, 120–137.

(21) Tantra, R.; Knight, A. *Nanotoxicology* **2010**, *2010*, 16.
(22) Lévy, R.; Shaheen, U.; Cesbron, Y.; Sée, V. *Nano Rev.* **2010**, *1*, 4889.
(23) Elsaesser, A.; Taylor, A.; de Yanes, G. S.; McKerr, G.; Kim, E. M.; O'Hare, E.; Howard, C. V. *Nanomedicine (London, U.K.)* **2010**, *5*, 1447–1457.
(24) de Jonge, N.; Peckys, D. B.; Kremers, G. J.; Piston, D. W. *Proc. Natl. Acad. Sci. U.S.A.* **2009**, *106*, 2159–2164.
(25) Ring, E. A.; de Jonge, N. *Microsc. Microanal.* **2010**, *16*, 622–629.
(26) Kingham, P. J.; Cuzner, M. L.; Pocock, J. M. *J. Neurochem.* **1999**, *73*, 538–547.
(27) Siegwart, D. J.; Srinivasan, A.; Bencherif, S. A.; Karunanidhi, A.; Oh, J. K.; Vaidya, S.; Jin, R.; Hollinger, J. O.; Matyjaszewski, K. *Biomacromolecules* **2009**, *10*, 2300–2309.
(28) Hui, S. W.; Parsons, D. F. *Science* **1974**, *184*, 77–78.
(29) Pierson, J.; Sani, M.; Tomova, C.; Godsave, S.; Peters, P. J. *Histochem. Cell Biol.* **2009**, *132*, 253–262.
(30) de Jonge, N.; Poirier-Demers, N.; Demers, H.; Peckys, D. B.; Drouin, D. *Ultramicroscopy* **2010**, *110*, 1114–1119.
(31) Ruan, G.; Agrawal, A.; Marcus, A. I.; Nie, S. *J. Am. Chem. Soc.* **2007**, *129*, 14759–14766.
(32) Bhattacharyya, S.; Bhattacharya, R.; Curley, S.; McNiven, M. A.; Mukherjee, P. *Proc. Natl. Acad. Sci. U.S.A.* **2010**, *107*, 14541–14546.
(33) Barua, S.; Rege, K. *Biomaterials* **2010**, *31*, 5894–5902.
(34) Neely, A. N.; Cox, J. R.; Fortney, J. A.; Schworer, C. M.; Mortimore, G. E. *J. Biol. Chem.* **1977**, *252*, 6948–6954.
(35) Vanlandingham, P. A.; Ceresa, B. P. *J. Biol. Chem.* **2009**, *284*, 12110–12124.
(36) Marquis, B. J.; Love, S. A.; Braun, K. L.; Haynes, C. L. *Analyst* **2009**, *134*, 425–439.
(37) Powers, K. W.; Brown, S. C.; Krishna, V. B.; Wasdo, S. C.; Moudgil, B. M.; Roberts, S. M. *Toxicol. Sci.* **2006**, *90*, 296–303.
(38) Tkachenko, A. G.; Xie, H.; Liu, Y.; Coleman, D.; Ryan, J.; Glomm, W. R.; Shipton, M. K.; Franzen, S.; Feldheim, D. L. *Bioconjugate Chem.* **2004**, *15*, 482–490.
(39) Brandenberger, C.; Muhlfeld, C.; Ali, Z.; Lenz, A. G.; Schmid, O.; Parak, W. J.; Gehr, P.; Rothen-Rutishauser, B. *Small* **1669**, *6*, 1669–1678.
(40) Weston, A. E.; Armer, H. E.; Collinson, L. M. *J. Chem. Biol.* **2009**, *15*, 15.
(41) Schrand, A. M.; Schlager, J. J.; Dai, L.; Hussain, S. M. *Nat. Protocols* **2010**, *5*, 744–757.
(42) Richard, J. P.; Melikov, K.; Vives, E.; Ramos, C.; Verbeure, B.; Gait, M. J.; Chernomordik, L. V.; Lebleu, B. *J. Biol. Chem.* **2003**, *278*, 585–590.
(43) Lundberg, M.; Johansson, M. *Biochem. Biophys. Res. Commun.* **2002**, *291*, 367–371.
(44) Wingard, C. J.; Walters, D. M.; Cathey, B. L.; Hilderbrand, S. C.; Katwa, P.; Lin, S.; Ke, P. C.; Podila, R.; Rao, A.; Lust, R. M.; Brown, J. M. *Nanotoxicology* **2010**, 3.
(45) Mayhew, T. M.; Muhlfeld, C.; Vanhecke, D.; Ochs, M. *Ann. Anat.* **2009**, *191*, 153–170.

■ NOTE ADDED AFTER ASAP PUBLICATION

This Letter was published ASAP on March 16, 2011. The ninth paragraph of the paper has been modified. The correct version was published on March 21, 2011.